Aerosol and Air Quality Research, 16: 593–605, 2016

ISSN: 1680-8584 print / 2071-1409 online
doi: 10.4209/aaqr.2015.05.0371

On the Transport of Urban Pollution in an Andean Mountain Valley

Ana María Cordova[1], Jorge Arévalo[1], Julio C. Marín[1*], Darrel Baumgardner[2], Graciela B. Raga[3], Diana Pozo[1], Carlos A. Ochoa[3], Roberto Rondanelli[4,5]

[1] *Departamento de Meteorología, Universidad de Valparaíso, Chile*
[2] *Droplet Measurements Technology, USA*
[3] *Centro de Ciencias de la Atmósfera, Universidad Nacional Autónoma de México*
[4] *Departamento de Geofísica, Universidad de Chile*
[5] *Center for Climate and Resilience Research, Santiago, Chile*

ABSTRACT

Urban pollution can often impact surrounding, non-urban regions, through advection and dispersal of pollutants by the prevailing winds. Urban regions located upstream of high mountains, such as the Andes, can potentially impact the cryosphere by deposition of particles onto the surface of the snowpack and glaciers.

Santiago, the capital of Chile, has more than 6 million inhabitants and regularly experiences episodes of severe pollution, particularly during the austral winter. Some studies have hypothesized that particle pollution from Santiago can reach the cryosphere downwind of the city, but the scarcity of measurements made high in the mountains prevents the validation of mesoscale models so the proof of actual impact remains elusive. A research project was designed to provide some insight into this question. The *Pollution Impact on Snow in the Cordillera - Experiments and Simulations* (*PISCES*) project was carried out in 2014 and includes both observational and modeling components. A five-week field campaign was conducted at the end of winter, at an elevated site in a mountain valley, 65 km to the southeast of the center of Santiago, to characterize some aspects of particulate pollution.

During synoptic conditions that result in clear days at the site, the mesoscale mountain-valley circulation is effective in transporting pollutants upwards during the day, leading to diluted particle concentrations beyond the summits of the highest peaks. Cloudy days with reduced up-valley circulation do not show increased concentrations associated with transport. Back trajectories indicate that air masses reaching the site during the field campaign are seldom influenced by pollution from Santiago.

Keywords: Andes cryosphere; Black carbon; Regional pollution; Mountain-valley circulations.

INTRODUCTION

There is overwhelming evidence that the continuing recession of glaciers worldwide is linked to climate change associated with human activities. Some studies (e.g., Ménégoz *et al.*, 2014) have indicated a role for black carbon (BC) particles that are deposited on the surface and accelerate localized melting of Himalayan glaciers. This is due to the absorption of solar radiation by BC particles that are heated and transfer this energy to the snow and ice. The BC particles seen in the Himalayas have been traced to anthropogenic emissions related to biomass burning, industrial processes and vehicular traffic.

In the Southern Hemisphere, the glaciers are also receding at an alarming rate (Baraer *et al.*, 2012; Rabatel *et al.*, 2013); however, very few studies have been carried out to determine whether the deposition of particles of anthropogenic origin is occurring over glaciers and the seasonal snowpack. Results from Cereceda-Balic *et al.* (2012) suggest that anthropogenic activities could be impacting the cryosphere in the Chilean Andes. Some recent measurements in the Peruvian Andes (Schmitt *et al.*, 2015) have reported increased concentrations of BC downwind of medium-sized urban areas located at an altitude (approximately 1500 m) lower than the sampled glaciers.

Santiago (33.46°S, 70.66°W, 542 m amsl) is the largest and one of the most polluted cities in Chile, with a population of about 6 million people (including the metropolitan region). Atmospheric pollution is a serious problem in the city, with concentrations of particulate matter less than 2.5 μm ($PM_{2.5}$) consistently exceeding the annual Chilean air quality standard of 20 μg m^{-3} (Jhun *et al.*, 2013). There is a large

* Corresponding author.
Tel.: +56 32 2508711
E-mail address: julio.marin@meteo.uv.cl

fleet of diesel-fueled buses in the city that contribute significantly to BC emissions. The pollution events, in terms of ambient concentration of particulate matter, are particularly serious during the austral winter (Gramsch *et al.*, 2014), when there are additional emissions present from domestic wood-burning for heating.

Santiago is located in the western foothills of the Andes Cordillera, and it has been hypothesized that pollution transported from the city can reach the high mountains, affect the regional environment and decrease the albedo of snow and glaciers. However, strong temperature inversions over Santiago during the winter lead to an accumulation of pollutants in the boundary layer that, on average, only reaches between 300 and 500 m in altitude (Muñoz and Undurraga, 2010). During the most intense pollution events, the winds are virtually calm in the basin where Santiago is located. Hence the question arises as to what mechanism can lead to the actual transport of pollution from the inversion-capped boundary layer of Santiago to the glaciers in the high mountains (c.a. 4500–5000 m amsl). Given the scarcity of measurements in the mountains, a research project was designed to address this question. The *Pollution Impact on Snow in the Cordillera - Experiments and Simulations (PISCES)* project was started in 2014 and includes both observational and modeling components. This project is part of a new initiative to evaluate the role of anthropogenic activities in the Andes, named *PISAC: Pollution and its impacts on the South American Cryosphere* (Molina *et al.*, 2015). The five-week field campaign was conducted during the months of September and October 2014 at an elevated site (1498 m amsl) in a narrow mountain canyon (Cajón del Maipo) located 65 km to the southeast of the center of Santiago. The objective of the field phase of PISCES was to characterize some aspects of particulate pollution and to identify its source and transport using simulations with a mesoscale model.

MEASUREMENTS AND ANALYSIS METHODOLOGY

The field campaign was conducted from 10 September to 15 October 2014 at Queltehues, a site located at 1498 m amsl close to the end of a narrow canyon, 65 km to the southeast of the center of Santiago. Fig. 1(b) shows the location of Queltehues within the complex topography at the western edge of the Andes cordillera and the nearby air-quality monitoring stations located in Santiago and its surroundings. The research site lies in a climatic transition zone between mild semi-arid Mediterranean and cold mountain climate. The site experiences a prolonged dry season, with maximum values of precipitation during the winter months and an annual mean value larger than 500 mm in the region (DGA, 2014). Winter temperatures can be below freezing at the site and some snow may accumulate at that altitude for a few days but does not remain on the ground throughout the winter.

The canyon is a popular region for tourists, particularly during summer, weekends and holidays, as was the case for the long-weekend of national Independence Day (18–21 Sept) during the period of the field campaign. There is also mining activity higher up in the valley and truck traffic, contributing to large concentrations of dust particles and BC from diesel fuel combustion.

Instrument Package

The measurement system included a meteorological station (Davis) and instruments for in situ sampling of the physical and optical properties of aerosol particles, a ceilometer to measure the vertical profile of aerosol particle backscattering and a web camera to record the view down the valley every 15 minutes. The total number concentration of condensation nuclei (CN) was measured with a TSI Model 3010 counter, the mass concentration of particle-bound polycyclic aromatic hydrocarbons (PPAH) with an Ecosystems PAS-1000 and the size distributions from 0.3 to 25 μm with a PMS LASAIR-300 (six size channels). The optical properties, i.e., the absorption and scattering coefficients, at 870 nm, were measured with the Droplet Measurement Technology (DMT) Photoacoustic Extinctiometer (PAX) and at 550 nm with a Radiance Research Nephelometer and Particle Soot Aerosol Photometer (PSAP), respectively. Equivalent black carbon (eBC) is derived from the absorption coefficients measured with the PAX and PSAP by applying an instrument and wavelength dependent specific absorption coefficient. Nakayama *et al.* (2015) and Retama *et al.* (2015) provide detailed information on the PAX and the PSAP is described by Bond *et al.* (1999). Vertical profiles of aerosol backscattering, with 20 m resolution, were measured with a Vaisala CL-31 ceilometer. The raw data were averaged in 300-second intervals for the analysis described below.

The solar radiation measurements at the site, as well as the ceilometer vertical backscatter profiles, were analyzed to select days mostly free of local clouds, i.e., when reductions occurred of only 10% of the maximum solar radiation for the time of year and site location. The rationale for this selection was to determine days when the diurnal cycle of the radiation-driven mountain-valley circulation would be strong. Only seven days: 30 September, 1, 2, 5, 6, 10 and 13 October qualified for this sub-group and the data from them were composited to obtain a typical diurnal variation when this mesoscale circulation was dominant.

Similarly, a total of 13 cloudy days (15, 22, 25–29 September and 4, 7, 8, 11, 12, 14 October), during which less than 90% of the maximum solar radiation was measured at the site, were included in this sub-group to determine the composite diurnal evolution. Cloudy days include partly cloudy conditions: no estimate was made of the time of the day nor of the length of time when clouds were present. These days were combined to evaluate the diurnal evolution when the mesoscale circulation was less strong than in clear days or not present. Even though the campaign was carried out during the transition between austral winter and spring, when synoptic scale disturbances bring precipitation to the Andes, only trace amounts of rain at the research site were recorded on 13 and 23 September and 5 October. These days are not included in the cloudy-day group. Separate consideration is given to a long weekend that coincided with the celebration of national Independence Day and during

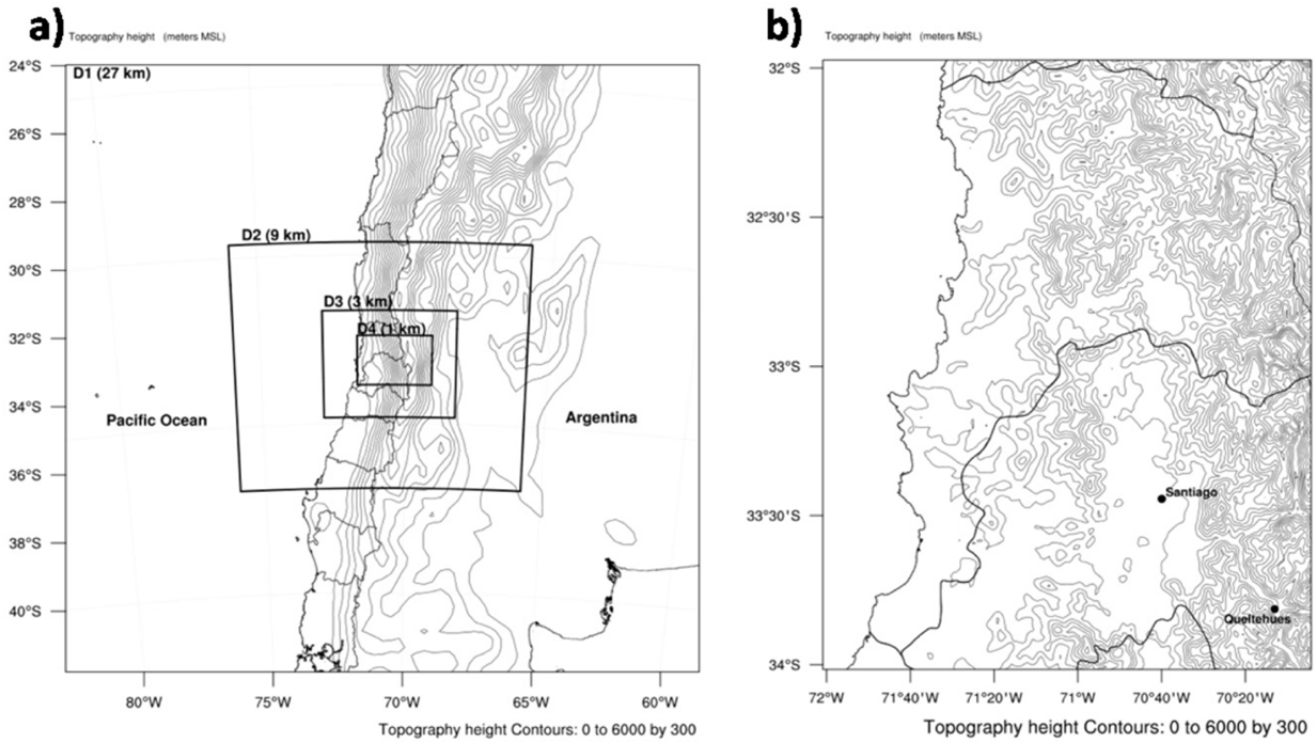

Fig 1. a) Computational domains for the simulations with WRF, with 27, 9, 3 and 1 km (D1, D2, D3, D4, respectively) horizontal resolution. b) Inner domain (D4) topography and observational sites. Contours show topography in both panels.

which time, large numbers of tourists visited the mountain valley and contributed to additional emissions from vehicles and from wood-burning used for grilling and heating.

A profound analysis of the large scale atmospheric conditions during the field campaign is beyond the scope of this paper since we focused on the local and regional features. However, a brief description of the composited synoptic conditions during cloudless and cloudy days provides useful context. Synoptic-scale variability was present in each of the two groups considered: cloudy and cloudless days. Despite this case-by-case variability, some noticeable differences were evident between the two groups. During cloudy days the center of the South Pacific Anticyclone was located further north than during cloudless days, while at mid-levels a trough was very clear with its axis located along the Chilean coast, favoring ascending motions over the Andes to the east. In contrast, a mid-level ridge was present during cloudless days, limiting upward motions over the mountains. At upper levels, the subtropical jet was located above the field site during cloudy days, showing stronger winds than during cloudless days.

WRF Model Configuration

The Weather Research and Forecasting (WRF) model is a numerical weather prediction system freely available that can be used for operational and research purposes (Skamarock *et al.*, 2008). A high horizontal resolution simulation was performed with Version 3.6.1 of the Advanced Research WRF core (ARW-WRF). Four model nested domains were employed in the simulation as depicted in Fig. 1(a), whose characteristics are shown in Table 1.

Only the results from the smallest domain (domain 4, D4), with the highest resolution, are discussed in this study. This domain covers an area of approximately 41000 km^2 that includes the Santiago metropolitan area, the coastal cities to the West and part of the Andes cordillera to the East, where the PISCES field site was located (Fig. 1(b)). The simulation employed the land-use data based on the Moderate Resolution Imaging Spectroradiometer (MODIS) land-cover classification of the International Geosphere-Biosphere Programme and modified for the NOAA land surface model at 30 arc seconds (approximately 0.9 km) in horizontal resolution.

The simulation included 60 vertical levels with variable resolution, with eight levels within the first kilometer in the vertical with spacing varying between 60 and 200 m. The model pressure top was 20 hPa and vertical damping was used at the upper boundary. The simulation was performed from 25th July to 15th October 2014, but only the days covering the PISCES period were analyzed here. Outputs from the simulation were stored every 1-h. The Climate Forecast System version 2 (CFSv2, Saha *et al.*, 2014) provided the initial and boundary conditions every 6 hours, and an analysis nudging was implemented in the outer domain (D1) to provide better boundary conditions during the simulation period.

The simulation used the RRTMG (Mlawer *et al.*, 1997) parametrization to calculate the shortwave and longwave radiations. The Tiedtke scheme (Tiedtke, 1989, Zhang *et al.*, 2011) was used to calculate convective processes in domains 1-3 and the WSM 6-class graupel scheme (Hong and Lim, 2006), a scheme with ice, snow and graupel processes

Table 1. WRF domains characteristics: *dx* and *nx* represent the horizontal resolution and number of points in the East-West direction, respectively; *dy* and *ny* represent the same in the North-South direction.

Domains	*dx* (*km*)	*Nx*	*dy* (*km*)	*ny*	Area ($\times 10^3$ km^2)
1	27	78	27	76	4322
2	9	94	9	109	829
3	3	127	3	148	169
4	1	181	1	229	41

suitable for high-resolution simulations, was used for microphysics. The Mellor-Yamada Nakanishi and Niino Level 2.5 parametrization (Nakanishi and Niino, 2006) was used for planetary boundary layer and surface layer processes and the Noah Land Surface Model (Chen and Dudhia, 2001) provided the soil temperature and moisture, the fractional snow cover and frozen soil physics.

RESULTS AND DISCUSSION

Aerosol Particle Properties

The ambient concentrations of 6-hour averages of CN (black line) and eBC (red line) are shown in Fig. 2(a), particle scattering coefficient (B_{scat}, black line) and PPAH (red line) in Fig. 2(b), and the vertical profile of the backscatter signal from the ceilometer in Fig. 2(c). The CN concentrations reflect the presence of very small particles, which typically do not contribute much to the scattering coefficient and could be associated with new particle formation. In urban settings, eBC and PPAH are highly correlated, since they are both primarily emitted by fossil-fuel combustion. Maximum values of CN concentrations above 2000 per m^3 and of particles with eBC of up to 1 μg cm^{-3} were observed only a few times during the campaign, also corresponding to higher values of PPAHs. The B_{scat} was observed to reach high values in several instances, sometimes not associated with the high CN, eBC or PPAH values, perhaps indicative of the presence of large dust particles. However, during most days the concentrations measured at the research site were much lower than those maximum values, as would be expected in a mountain environment away from major urban sources. Local sources can contribute to the large concentrations and also mesoscale processes can transport pollution from the urban areas further away and impact the research site.

Composite of Cloudless Days

Predominantly cloudless days (30 September, 1, 2, 5, 6, 10 and 13 October) during the field campaign were composited to evaluate pollution characteristics when the mesoscale mountain-valley circulation was present.

Fig. 3(a) shows the diurnal evolution of the 1-hour averages of temperature and relative humidity for the composite clear days. Note that an average 10°C diurnal temperature amplitude was observed and that the relative humidity ranged from a maximum of 40% during the night and early morning hours to about 10% at 15:00–16:00 LT (LT = UTC - 3). The winds (Fig. 3(b)) were very consistent in speed and direction; lower magnitudes (3–4 m s^{-1}) were observed during the night and early morning and then started to increase at about 11:00–12:00 LT. An average maximum speed of 12 m s^{-1} was observed between 14:00 and 15:00 LT. The variability in wind speed is represented by the standard deviation and indicated by the vertical bars in Figs. 3(b) and 3(d). The wind direction was quite consistent, southerly during the night and early morning hours (downslope at the research site) and northerly during the day (up-valley).

The corresponding diurnal cycle of some of the particle properties are shown in Fig. 4 for clear, cloudy and holidays. The CN number concentrations (black line in Fig. 4(a)) are very small during the night up to local noon, when the wind shift occurs at the site during clear days. The concentrations (600–700 cm^{-3}) are very low, representative of pristine continental regions. Later in the afternoon, the northerly, up-valley flow transports air with much higher concentrations that, on average, almost reach 2000 cm^{-3}. In contrast, the scattering coefficient (red line in Fig. 4(a)) shows very little diurnal variability, with comparable values throughout the day, and only a minimum at mid-day coinciding with the minimum in CN associated with the shift in wind direction and the increase in wind speed. Note that this apparent lack of correlation in the afternoon is related to the fact that the B_{scat} represents the contribution of the scattering of light (at 910 mm) by particles and is a function of the surface area of the particles and the number concentration, whereas the CN measurements can be associated with new particle formation, with very small sizes, that make a small contributions towards the total scattering coefficient.

There is very little diurnal evolution of the eBC concentrations shown in Fig. 4(d) (black line), with a slight minimum around local noon and larger concentrations during the afternoon. It is interesting to note that the eBC concentration (and B_{scat} to a lesser degree) indicates a peak between 6:00 and 7:00 LT, a likely result of a local source, perhaps associated with wood-burning, local diesel traffic and even some resuspension of dust on unpaved mountain roads. There are very low concentrations of PPAH in the particles observed at the research site (red line, Fig. 4(d)) and almost no discernible diurnal cycle. There is a moderate correlation between eBC and PPAH at the site (correlation coefficient = 0.5, significant to $P < 0.01$), to be expected since both parameters are associated with emissions from engines using diesel fuel. There appears to be an unexplained time delay of about 1 hour (on average) in the maximum value of PPAH in the morning after the observed peak of eBC.

The composite vertical profile of backscatter (Fig. 5(a)) confirms the low B_{scat} values observed at the surface as the wind speed starts to increase and the wind direction shifts

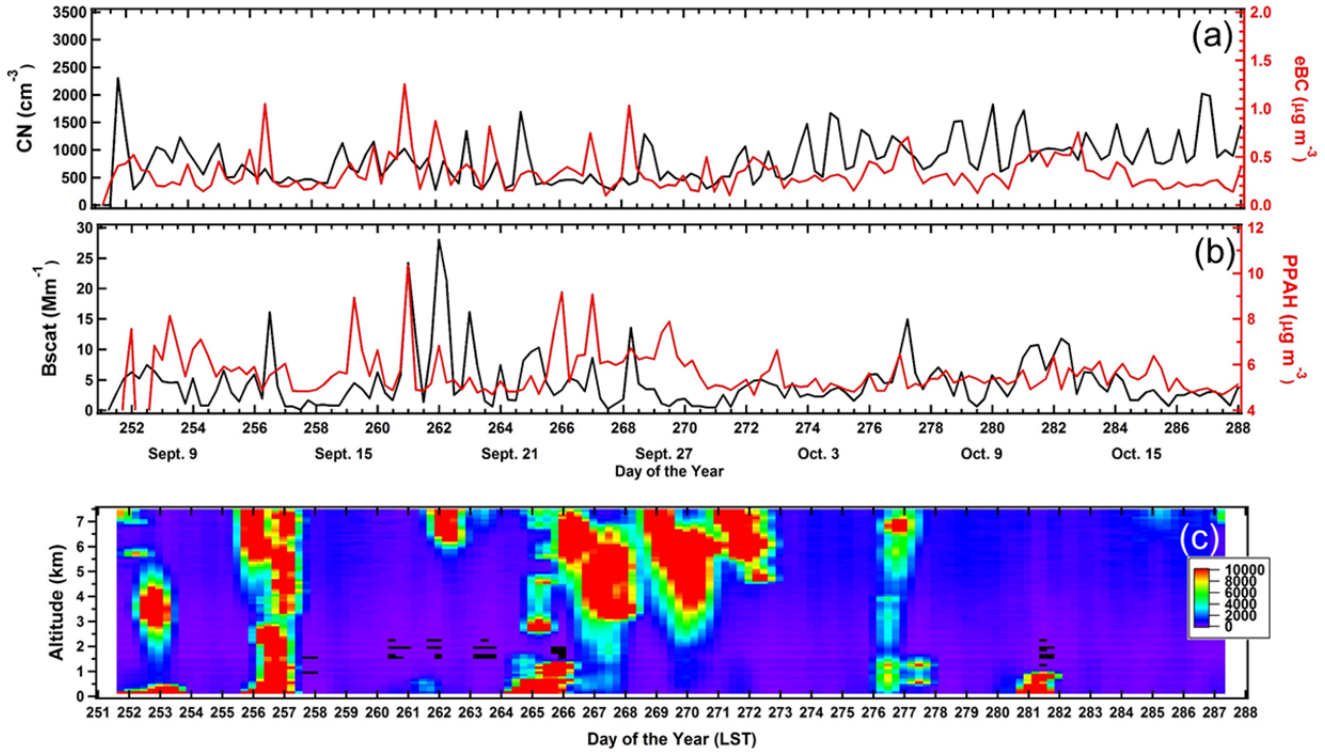

Fig. 2. Time series over the whole period of the field campaign for 6-hour averages of: a) condensation nuclei (CN, black line) and equivalent black carbon determined by the PAX (eBC, red line); b) particle scattering coefficient (Bscat, black line) and particle-bound polycyclic aromatic hydrocarbons (PAH, red line); and c) vertical profile of particle backscatter.

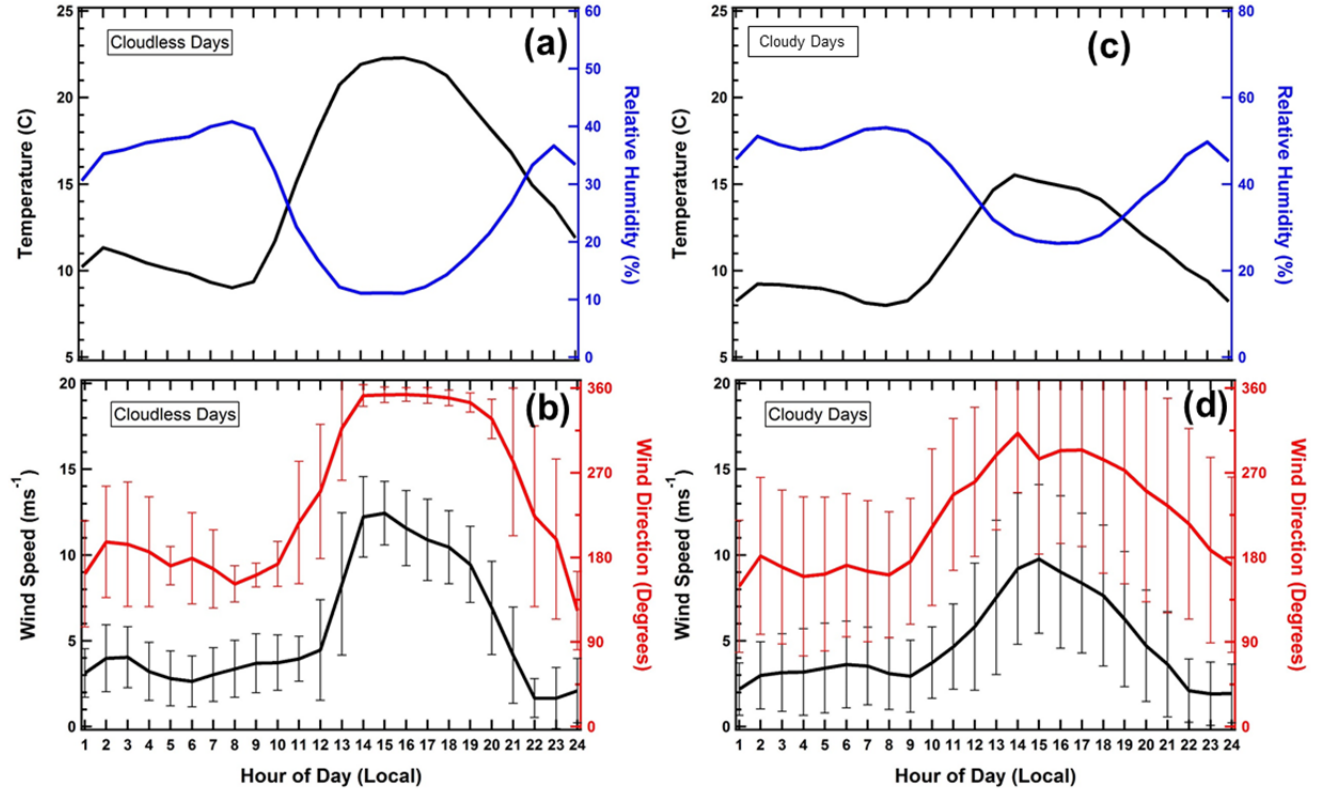

Fig. 3. Composite diurnal evolution of temperature (black line) and relative humidity (blue) for a) cloudless and c) cloudy days and wind speed (black line) and direction (red) for b) cloudless and d) cloudy days. Vertical bars are ± one standard deviation.

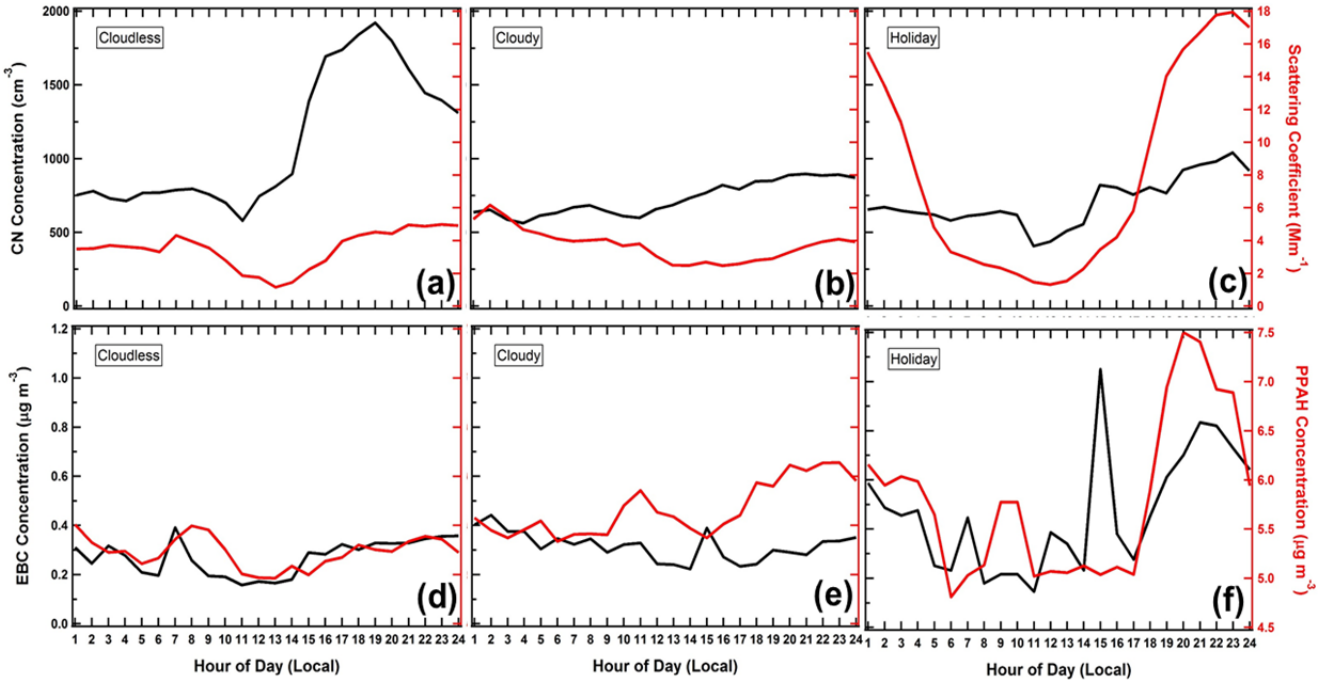

Fig. 4. Composite diurnal evolution of CN concentration (black line) and Bscat (red) for a) cloudless days, b) cloudy days and c) the national holiday and composite diurnal evolution of PAX eBC mass concentration (black line) and PPAH mass concentration (red) for d) cloudless days, e) cloudy days and f) holiday days.

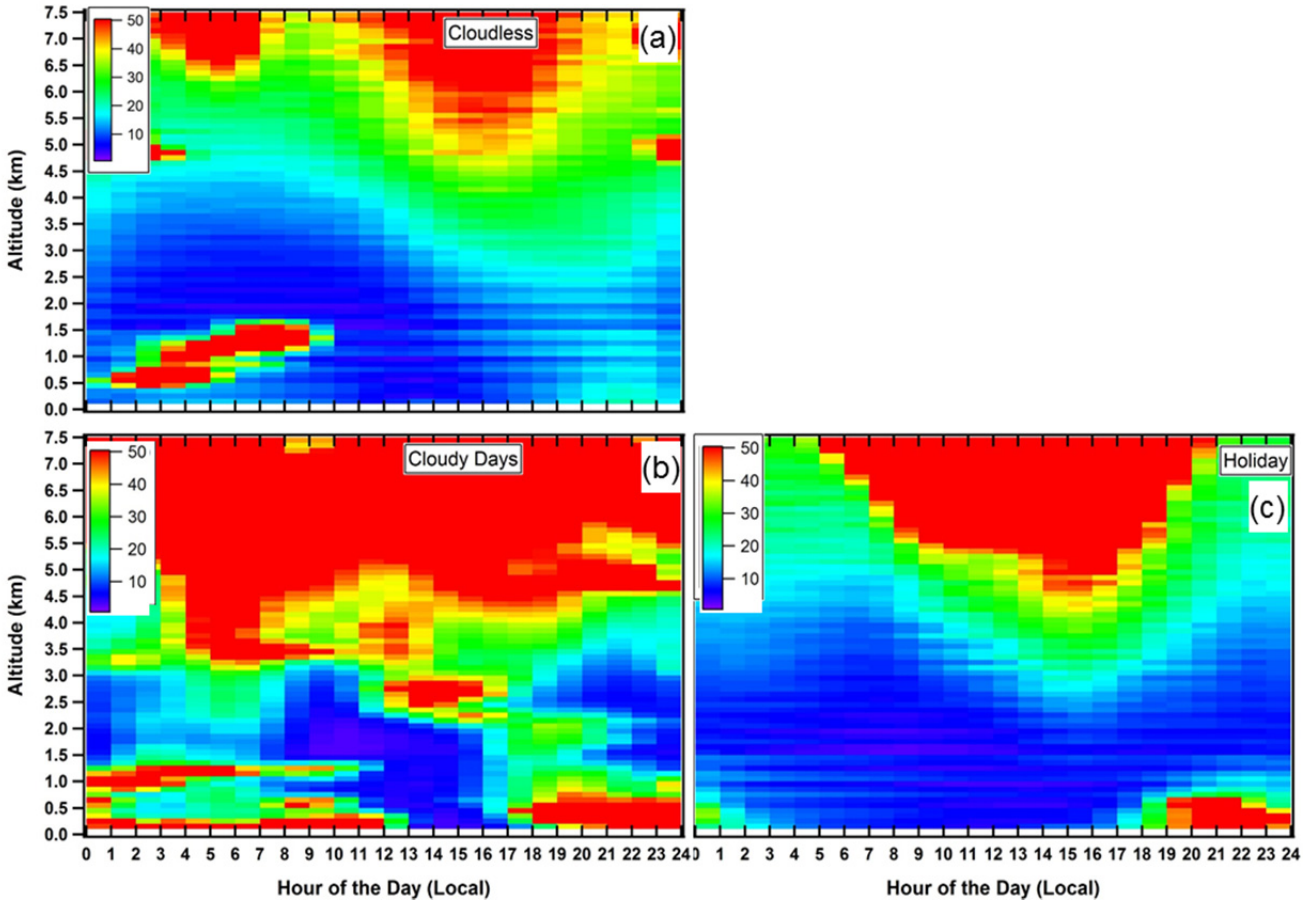

Fig. 5. Composite diurnal evolution of the vertical profile of the backscatter signal detected by the ceilometer for a) cloudless days, b) cloudy days and c) the national holiday.

to northerly (up-valley). It also shows a diluted vertical layer of aerosols (extending up to 1.5 km above the research site) when the surface measurements show peaks in particle properties between 19:00 and 21:00 LT. There is a layer of aerosols above the site during the early morning hours (between 1:00 and 8:00 LT) that rises from 500 m to 1.5 km over time. This elevated feature is perhaps related to recirculation of the aerosols dispersed upwards during the afternoon, but the magnitude appears much larger, so it has to include aerosols from other regions or perhaps even some thin clouds that may have developed during the night above the research site. A most remarkable, consistent feature is observed several kilometers above the research site: there is moderate particle backscatter in regions from 5 to 7 km that appears to indicate a strong diurnal cycle. Note that the heights at which this backscatter is observed are above the highest peaks of the Andes at this latitude. It could be perhaps associated with the presence of very thin or sub-visible cirrus clouds that did not substantially reduce the solar radiation at the site.

The dispersion diagram between CN and eBC concentrations for the clear days (Fig. 6(a)) shows two separate groups of points. The group with higher CN values correspond to the afternoon observations, after the up-valley circulation has been established, and is indicative of a different population from the early morning-to-midday observations. In contrast, Fig. 6(d) shows the expected correlation between eBC and PPAH during the clear days (correlation coefficient = 0.5, significant to $P < 0.01$), related to a common emission source. This difference in the behavior of these variables (CN-vs-eBC) and (PPAH-vs-eBC) is noteworthy since in urban regions all these parameters are typically very well correlated when the main emission sources are associated with the transportation sector. The higher CN values observed during the upslope flow in the afternoon are not correlated with eBC or PPAH and hence are likely not originating from the combustion of diesel fuel. The correlation seen between eBC and PPAH would indicate that both have originated from the combustion of diesel fuel, but not necessarily transported by the up-valley flow.

Composite of Cloudy Days

A total of 13 cloudy days (15, 22, 25–29 September and 4, 7, 8, 11, 12, 14 October) were included in this sub-group to determine the composite diurnal evolution. The evolution of the 1-hour averages of temperature and relative humidity (Fig. 3(c)) is somewhat different than for the composite of clear days (Fig. 3(a)). The diurnal temperature amplitude was smaller due to less available solar radiation and the relative humidity was somewhat larger during the mid-day period when the minimum was observed. Little variation was observed during the nighttime between the two composites. Lower wind speeds (3–4 m s^{-1}) were observed on average during the night and early morning on cloudy days compared

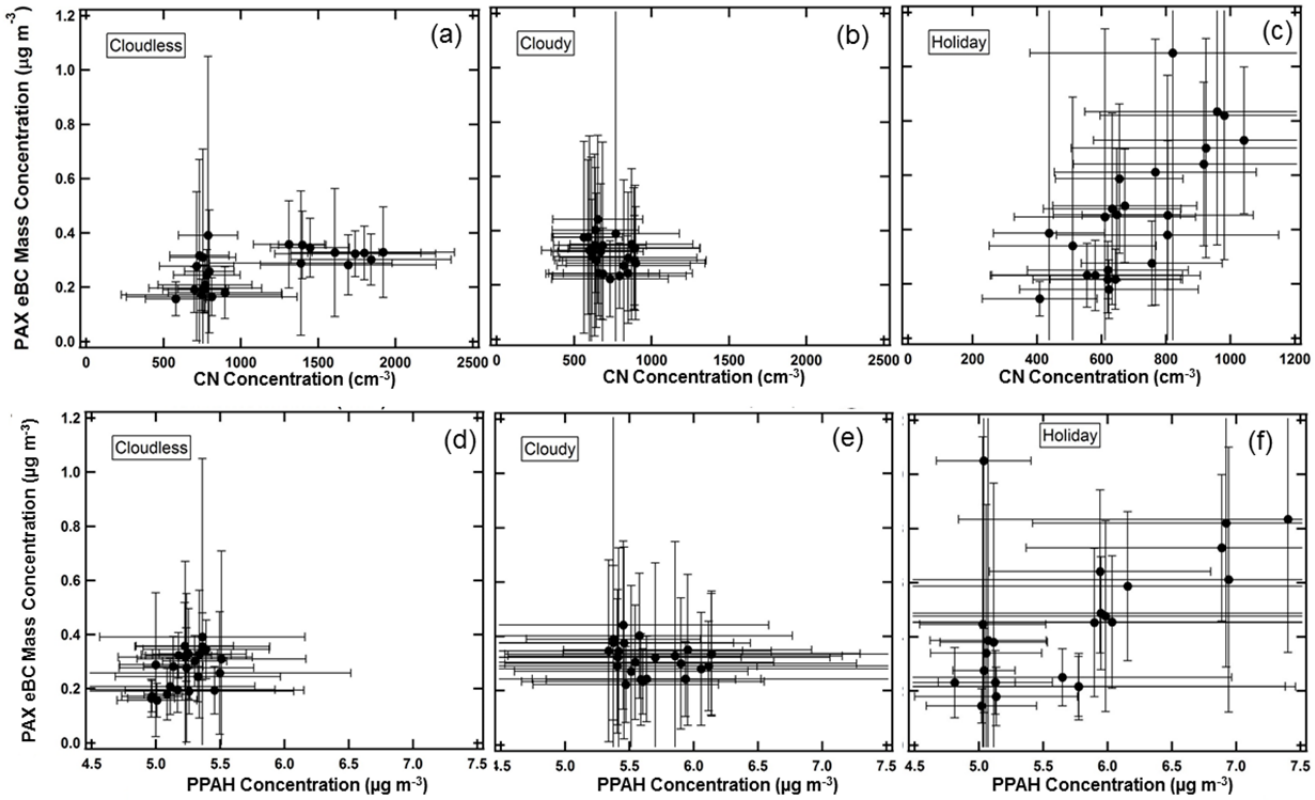

Fig. 6. The relationship between the PAX derived eBC mass concentration and CN number concentration are shown for a) cloudless days, b) cloudy days and c) the national holiday. The relationship between the PAX derived eBC mass concentration and PPAH mass concentration are shown for d) cloudless, e) cloudy and f) holiday days. The vertical and horizontal bars represent ± one standard deviation.

to clear days and maximum values were about 30% lower on cloudy days (Fig. 3(d)). The largest difference between clear and cloudy days was seen in the wind direction. While the flow in the afternoon was northerly on clear days, corresponding to up-valley, winds on cloudy days were closer to westerly during the afternoon and exhibited more variability. This difference in the wind direction during the afternoon, between clear and cloudy days, is fundamental in explaining the differences in the composites of aerosol characteristics observed at the site between these two sub-groups.

The CN number concentration (black line, Fig. 4(b)) and scattering coefficient (red line, Fig. 4(b)) were significantly different in cloudy days compared to clear days (Fig. 4(a)). There was no evident diurnal cycle in these variables on cloudy days. The clear day maximum in CN, observed in the afternoon during the up-valley flow (Fig. 4(a)) was absent on cloudy days, when the flow had a more westerly component and therefore, did not transport particles from lower in the valley. There is no correlation in the diurnal evolution of eBC concentration (black line) and PPAH (red line) during cloudy days (Fig. 4(e)), as compared to clear days. It is particularly surprising to see that the PPAH reached a maximum in the late evening at the research site and was not associated with an increase of eBC.

The composite vertical profile of backscatter signal determined by the ceilometer does not show a diurnal cycle on cloudy days (Fig. 5(b)). Several layers of backscatter signals are shown in the vertical, associated with the average cloudiness during the days included in the composite.

On cloudy days, when there is no up-valley circulation in the afternoon, the dispersion diagram between CN and eBC concentrations (Fig. 6(b)) does not show a significant bimodal distribution, which is evident on clear days (Fig. 6(a)). In contrast, Fig. 6(e) shows a distinct separation between eBC and PPAH on cloudy days, which is related to the afternoon higher PPAH concentrations shown in Fig. 4(e) that are uncorrelated with the eBC.

Long-Weekend during National Independence Day

The research campaign started before the long weekend during the celebration of Independence on 18 and 19 September that attracted many tourists to the mountain valley. The observations at our research site indicate that tourists were already arriving on 16 September, since mass concentrations of eBC were much higher than previous and later days in the sample. Therefore, a composite diurnal cycle was derived with 5 days (16 through 20 September) influenced by local sources. As for clear and cloudy days, the graphs depicting the diurnal evolution of particle properties are shown in Figs. 4(c) and 4(f). Note that the afternoon peak in CN associated with up-valley flow (black line, Fig. 4(a)) was not present during the holidays (black line, Fig. 4(c)) whereas the scattering coefficient (red line, Fig. 4(c)) was about a factor of 3 larger than the typical up-valley situation (red line, Fig. 4(a)). Much larger values of eBC (black line, Fig. 4(f)) and PPAH (red line, Fig. 4(f)) were also observed in this composite during the holidays (compared with values in Fig. 4(d)). The vertical profile from the ceilometer (Fig. 5(c)) clearly indicates the presence of an aerosol layer close to the surface from 17:00 LT and extending beyond midnight associated with local sources. The dispersion diagrams between eBC and CN and eBC and PPAH (Figs. 6(c) and 6(f)) show higher correlations between these variables that are being emitted by local sources within the valley. The correlation coefficient between eBC and PPAH during these days is 0.6, higher than the 0.5 value for cloudless days (both with $P < 0.01$). These observations at the research site up the valley 65 km SE from Santiago are not consistent with observations made with the same instrumentation in other large urban areas such as Mexico City and Buenos Aires. The signature of predominantly vehicular emissions, common to all large urban centers, is not evident in the observations up the valley where there was the expectation to observe the regional transport of pollutants from Santiago. The afternoon peak in CN is not seen in B_{scat}, eBC nor PPAH, which indicates that the very small particles measured are not associated with vehicular emissions. Other sources in the valley, most likely from gas-to-particle conversions perhaps of biogenic origin, would be associated with this afternoon increase during the cloudless days.

Ceilometer Data Downtown in Santiago

Historical records of ceilometer measurements in Santiago (Muñoz and Undurraga, 2010) show that the wintertime boundary layer is typically only 300–500 m deep; the same equipment was in operation during the PISCES field campaign. In Santiago, the ceilometer has operated since March 2007 on the roof (15 m above ground level) of the Department of Geophysics Building, close to downtown. Figs. 7(a)–7(h) show the vertical profiles of backscattering for 1 and 2 October (Figs. 7(a) and (b)) and October 11 and 12 (Figs 7(e) and 7(f)). Visible camera images taken at the research site show clear conditions on 1 and 2 October, and cloudy conditions on 11 and 12 October. Note that the boundary layer in Santiago is very shallow all four days (maximum heights less than 500 m), and moreover, that there are no obvious differences in the ceilometer profiles on the clear or cloudy days observed at the Queltehues site.

Mesoscale Circulations

The composite of 10 m winds for clear days from the WRF simulations is shown in Fig. 8 together with the model topography at 15:00 LT, when the wind speed maximum is observed at the research site. Near-surface simulated winds flow within the narrow canyon and uphill over the topography, resulting in the up-valley circulation suggested by the observations. Note that this up-valley and up-slope flow reaches the research site from the NNW in agreement with observations (Fig. 3(b)). At night, the downslope flow is established and winds are from the SSE at the research site (not shown).

Vertical cross sections at the location of the research site are analyzed to explore the vertical extent of the diurnal mesoscale up- and down-valley circulations. Composites of vertical velocity (isolines) and equivalent potential temperature (color shaded) for clear and cloudy days at

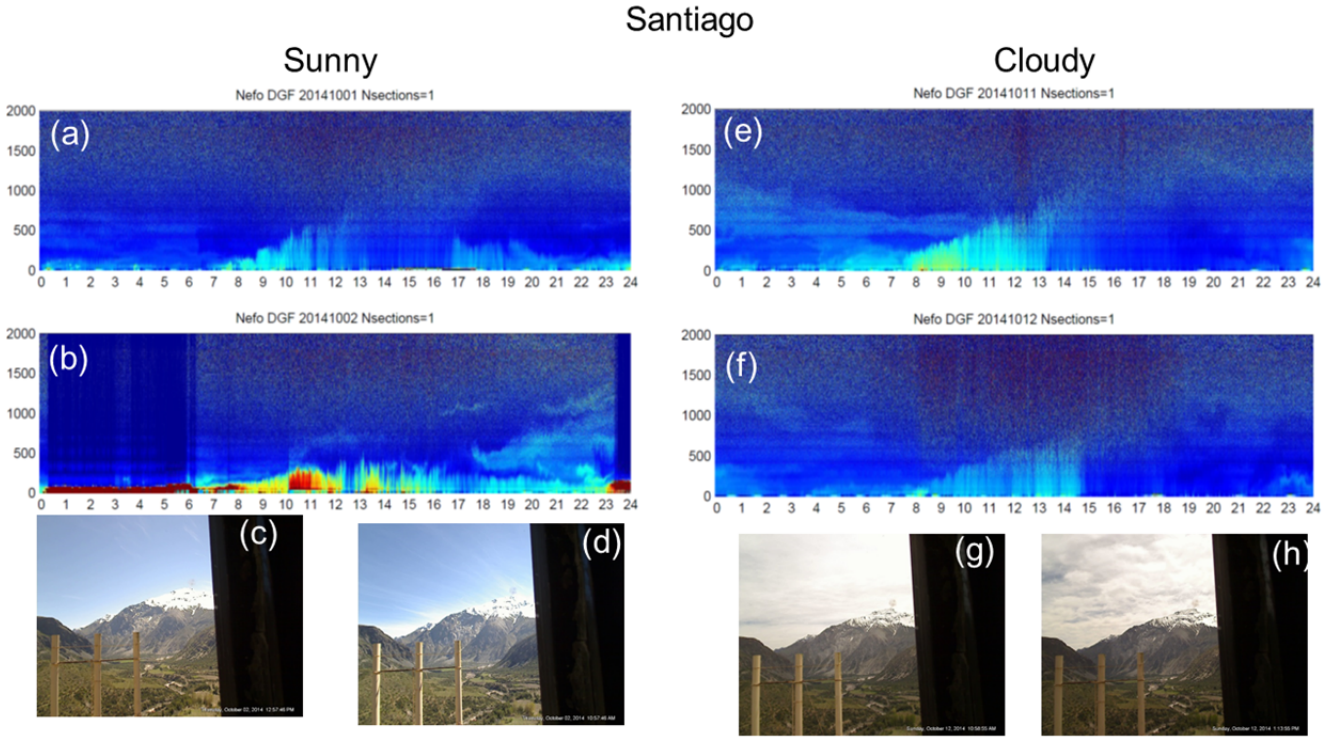

Fig. 7. Vertical profile of particle backscatter from the ceilometer located at downtown Santiago for a) 1 October, b) 2 October, e) 11 October and f) 12 October. Visible images captured at the field site at shown for the same days on c), d), g) and h), respectively.

15:00 LT are shown in Figs. 9(a) and 9(b), respectively. This plane (red line in Fig. 8) is perpendicular to the direction of the main near-surface winds during the afternoon. On clear days, a well-mixed air mass is observed over the mountain slope where the field site is located, co-located with positive vertical velocities. Surface heating gives rise to convective motions and turbulence in the valley and contribute to the mixing; the top of the well-mixed boundary layer is seen at about 2 km above the surface. Note the compensating downdrafts over the higher topography on each side of the valley. This vertical cross section clearly shows the up-valley and up-slope circulation that was inferred from the aerosol observations at the site. During cloudy days (Fig. 9(b), also at 1500 LT), there is evidence of the up-valley and up-slope circulation, but the vertical extent is more limited than on clear days (the top is less than 1.5 km above the surface), due to the reduce trajectories and correspond to about 50% of all trajectories. It shows that air masses arriving at the Queltehues site come mostly from rural areas surrounding Santiago city to the SW and then across the canyon at a height around 500 m agl. Air masses following these trajectories would not be directly in contact with the polluted central Santiago region. In fact, they would be in contact with pollutants characteristics of the southern periphery of Santiago, where other studies have indicated (Seguel *et al.*, 2013; Gramsch *et al.*, 2014) that the air quality is not correlated with conditions in Santiago and sometimes even considered more representative of background aerosol concentrations. A detailed analysis of the individual trajectories in this cluster indicates arrival at the research site mainly between 1800 LT and 0300 LT. Recall that CN concentrations reached a maximum at the research site at 18:00 LT (Fig. 4(a)). A second cluster indicated by the dark blue line in Fig. 10(a), corresponds to 42% of all trajectories and it traverses the Andean Foothills SE of Santiago. The wind speeds in this cluster are much lower than in the first cluster and that is why this line is shorter in the graph even though it also covers 18 hours. These trajectories do not even initiate near Santiago and it is unlikely that the air masses would be affected by pollution from the city. The trajectories in this cluster arrive at the research site between 06:00 and 12:00 LT and would not contribute to the observed peak in CN during the late afternoon at the research site. The third cluster indicated by the orange line in Fig. 10(a)) represents only 8% of all trajectories and although there is an indication that they go over the NW sector of Santiago, their altitude is at about 1000 m agl. As shown in Fig. 7, the average mixed layer height observed in Santiago is lower during those clear days, so in fact the air masses with trajectories in this cluster would not be in contact with the polluted boundary layer over the city.

Three trajectory clusters were also calculated for cloudy days, to evaluate differences from those just discussed for clear days. A first cluster indicated by the light blue line in Fig. 10(b) represents 57% of all trajectories. It shows trajectories going through rural areas south of Santiago and through Cajón del Maipo between 300 m and 500 m agl. The main difference between the largest cluster in clear days, is the initiation further west on cloudy days. The second

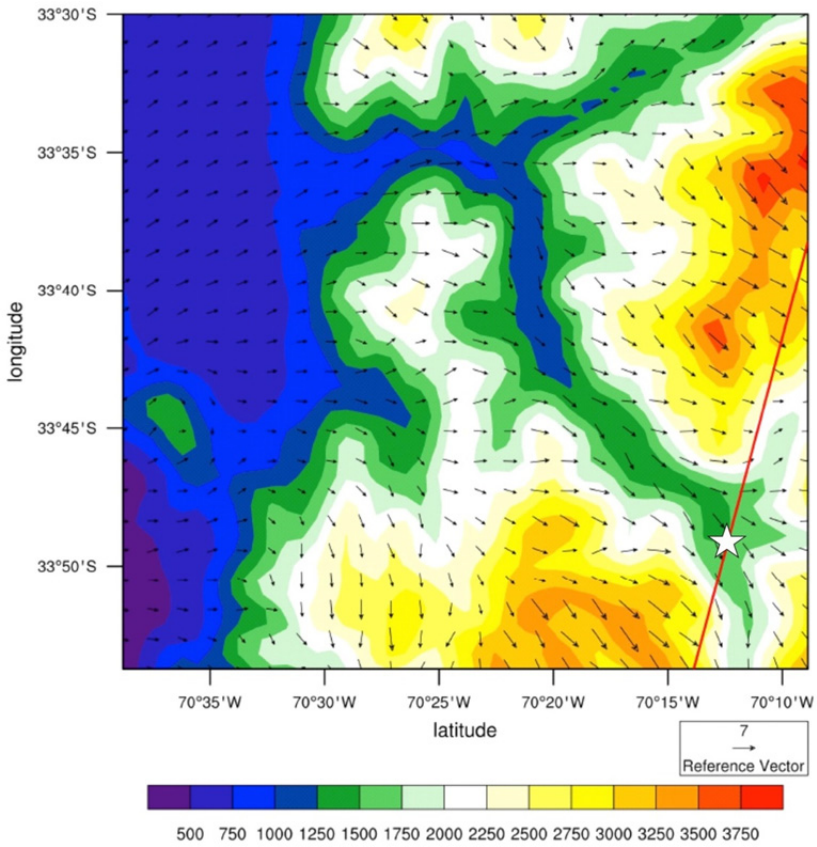

Fig. 8. Horizontal plane of composite 10 m wind vectors for clear days superposed on the WRF terrain. The diagonal line shows the location of the vertical cross section shown in Fig. 9. The white star shows the location of the field site.

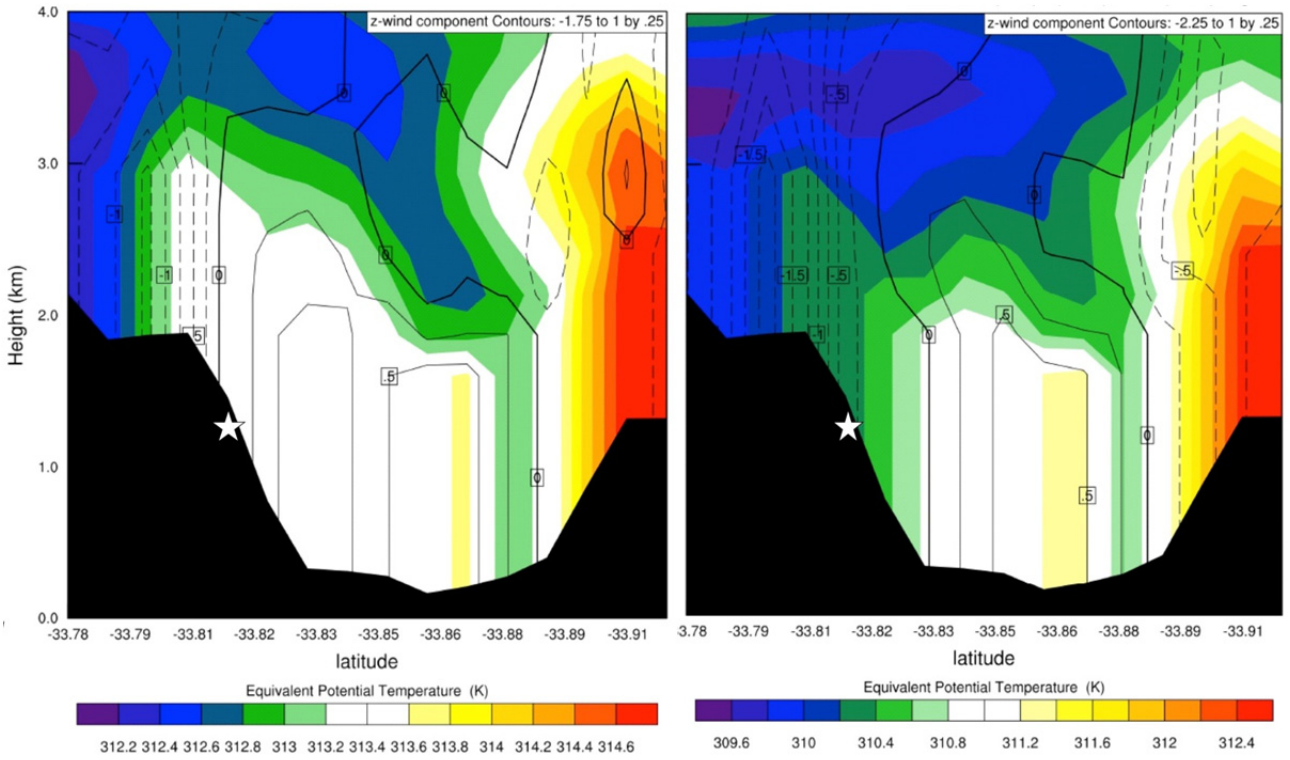

Fig. 9. Vertical cross section (diagonal line in Fig. 8) of composite equivalent potential temperature (shaded color) and vertical velocity (isolines) for (a) clear days and (b) cloudy days superimposed on the WRF terrain. The white star shows the location of the field site.

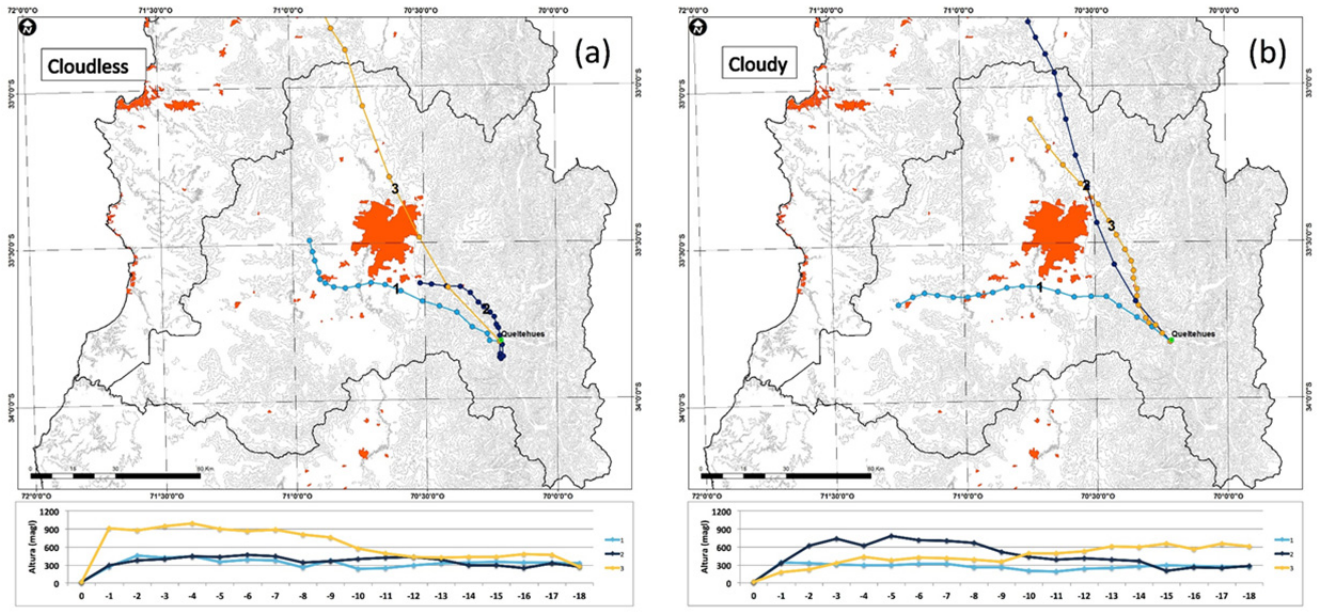

Fig. 10. Hysplit backtrajectories for (a) clear days and (b) cloudy days.

cluster represented by the dark blue line in Fig. 10(b) corresponds only to 11% of all trajectories, and shows a trajectory from the north over the Andean Foothills to the east of Santiago, between 700 m and 800 m agl. Air masses in this cluster of back trajectories would not be in contact with the polluted boundary layer in Santiago. The third cluster (orange line in Fig. 10(b)) represents 32% of all trajectories, and it shows an average trajectory coming from the N of Santiago, at a height of approximately 600–700 m agl, again typically above the polluted boundary layer over Santiago. The time of arrival of trajectories for cloudy days shows more variability than those calculated for cloudless days, perhaps associated with larger variability of the synoptic conditions. Most trajectories arriving at the research site between midnight and 09:00 LT belong to the first cluster, while those arriving between 12:00 and 18:00 LT are included in the third cluster. Recall that the observations do not show a diurnal cycle during cloudy days and none of the trajectories would bring polluted air to the research site. So, these modeling results are very consistent with the conclusion derived from observations that there appears to be no influence of aerosol pollution from Santiago at the research site.

SUMMARY AND CONCLUSIONS

A five-week field experiment was conducted at an elevated site in a mountain valley 65 km SE of Santiago, Chile, to measure physical and optical properties of aerosol particles and assess the potential impact of pollution from Santiago on the Andean cryosphere.

The observations indicate a significant difference in the diurnal cycle of CN concentrations between cloudless and cloudy days, with a peak in concentrations only seen at the research site on cloudless days at about 18:00 LT. The relation between CN concentrations and the solar radiation measured during the whole field campaign (Fig. 11) is a good summary for the conditions seen at the research site. Very clean conditions are present during cloudy days while the cloudless days show maximum concentrations during the late afternoon. Together with the sharp changes in wind direction under cloudless conditions, these observations are indicative of a mesoscale wind circulation driven by surface heating with up-valley and upslope flow during the day and downslope flow at night. This circulation is not inferred from the aerosol observations under cloudy conditions, due to the reduced surface forcing. The high-resolution simulations with the WRF model show the presence of the up-valley and upslope circulation during cloudless and cloudy days. However, only during cloudless days is the circulation strong enough to reach the location of the research site. The vertical extent of this circulation is reduced on cloudy days. These modeling results are very consistent with the aerosol observations. Moreover, the analysis of back trajectories from the research site for 18 hours, indicates that during the field campaign none of the air masses reaching the research site were from the polluted boundary layer of central Santiago.

The aerosol observations at the research site up the valley 65km SE from Santiago are not consistent with observations made with the same instrumentation in other large urban areas such as Mexico City and Buenos Aires, i.e., the signature of predominantly vehicular emissions, common to all large urban centers, is not evident in the observations up the valley where there was the expectation to observe the regional transport of pollutants from Santiago. This somewhat unexpected result deserves much further research with mesoscale modeling coupled with chemical processes to understand the nature of the peak in CN concentrations observed in the late afternoon at the research site.

Atmospheric conditions during the field project were typical of that shown at the end of the winter season. The

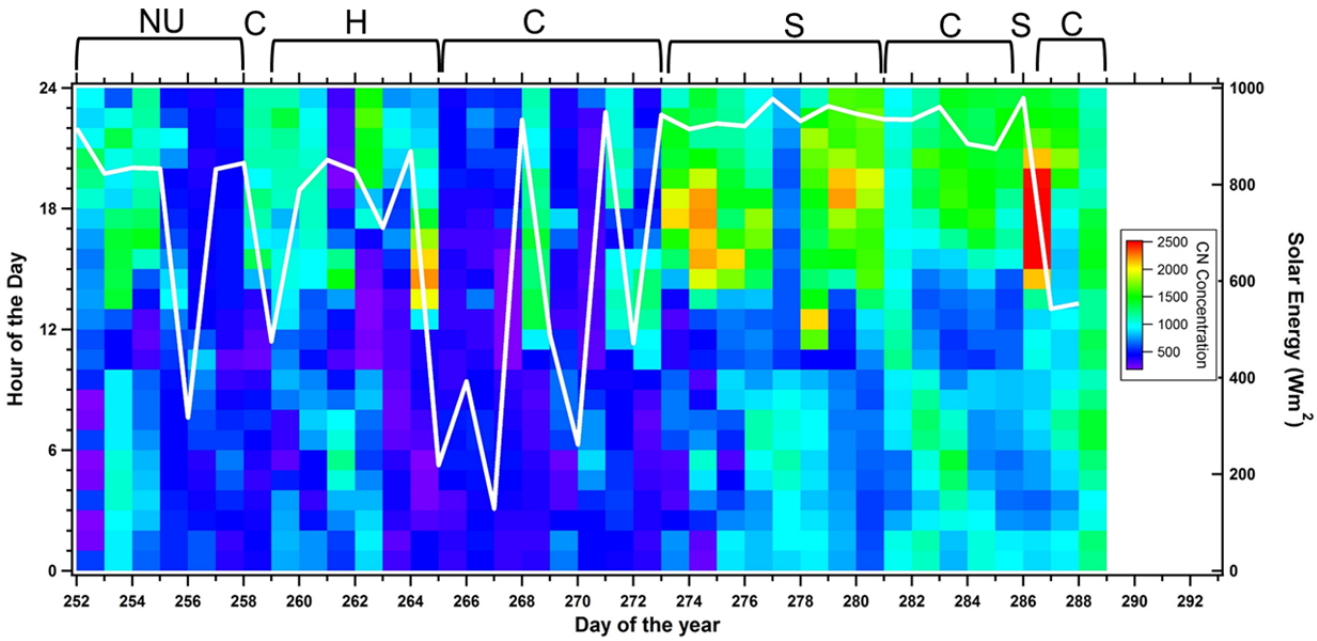

Fig. 11. The average hourly CN number concentrations are shown here as a function of the day of the year during the field experiment (shaded color). The white curve is the daily maximum solar radiation. The letters along the top of the figure mark the analyzed periods: NU - Not used; C - Cloudy; S - Sunny and H - Holiday.

atmospheric mixed layer height during winter months in the Santiago basin reaches only up to 600m at midday and early afternoon hours (Fig. 7 in Muñoz and Undurraga, 2010). There are winter-time episodes like the passage of frontal systems that can provide a synoptic environment favorable for the atmospheric boundary layer to surpass 1 km height, providing the ventilation of the city. Larger mixed layer heights are observed during late spring and summer months (November–February), where atmospheric boundary layer heights near and above 1 km are more frequent.

Only a single case of a cut-off low and one case of a frontal system passage occurred during the field campaign. Work is currently underway to study whether they caused a much different impact on the field site than that shown in this paper. Similar studies should be conducted in summer months to analyze whether pollution from Santiago can reach higher altitudes in the Andes that could impact negatively the cryosphere. Nevertheless, during summer most of the yearly snowpack melts and provides fresh water to cities and agricultural activities on both sides of the Andes. The exposed soil is a source of mineral dust particles that deposit over the glaciers and also affect the local radiative balance (Schmitt *et al.* 2015).

Studies, such as that of Quiroz *et al.* (2009), have shown the presence of anthropogenic pollution in the Aconcagua valley, which is located very close to the main highway that links Chile and Argentina, with very large flow of trucks, buses and cars, throughout the year. During winter, it is visually evident that black carbon and dust particles associated with traffic deposit over the snow in the ski resort of Portillo, on the Chilean side. During summertime, Seguel *et al.* (2013) indicate that regional transport of polluted air from the lowlands is likely to occur up to the Aconcagua valley. The measurements in our field campaign, to test the hypothesis that the pollution from Santiago could reach high altitudes during winter, were made up at a different valley (not the one with the busy highway), in order to avoid the clear influence of the vehicles that emit particles high up in the Andes.

Another source of vehicular pollution at high altitudes is associated with the mining industry, as has been demonstrated by Cereceda-Balic *et al.* (2012), but again, the sources are high up within the Andes and do not originate in the lowlands where the large urban centers are located.

ACKNOWLEDGMENTS

Universidad Nacional Autónoma de México (UNAM) is gratefully acknowledged for covering the costs of transportation of the equipment from Mexico City to Chile and for support during the fieldwork. JCM acknowledges the project Fondecyt 11121473 for support. RR acknowledges support from the Center for Climate and Resilience Research, CONICYT/FONDAP/15110009. Powered@NLHPC: This research was partially supported by the supercomputing infrastructure of the National Laboratory for High Performing Computer (NLHPC) (ECM-02). The Climate Forecast System v2 were provided by the Research Data Archive at the National Center for Atmospheric Research, Computational and Information Systems Laboratory. Ricardo Muñoz is gratefully acknowledged for providing the ceilometer pictures used to create Fig. 7. Special thanks are due to AES Gener for approval of the use of the site to carry the field campaign and for logistical support. F. Cereceda-Balic is gratefully acknowledged for his collaboration on site selection and coordination with AES Gener.

REFERENCES

Baraer, M., Mark, B.G., McKenzie, J.M., Condom, T., Bury, J. Huh, K., Portocarrero, C., Gomez, J. and Rathay, S. (2012). Glacier Recession and Water Resources in Peru's Cordillera Blanca. *J. Glaciol.* 58: 134–150.

Bond, T.C., Anderson, T.L. and Campbell, D. (1999). Calibration and Intercomparison of Filter-Based Measurements of Visible Light Absorption by Aerosols. *Aerosol Sci. Techonl.* 30: 582–600.

Cereceda-Balic, F., Palomo-Marín, M., Bernalte, E., Vidal, V., Christie, J. Fadic, X., Guevara, J.L., Miro, C. and Pinilla Gil, E., (2012). Impact of Santiago de Chile Urban Atmospheric Pollution on Anthropogenic Trace Elements Enrichment in Snow Precipitation at Cerro Colorado, Central Andes. *Atmos. Environ.* 47: 51–57.

Chen, F. and Dudhia, J. (2001): Coupling an Advanced Land Surface–Hydrology Model with the Penn State–NCAR MM5 Modeling System. Part I: Model Implementation and Sensitivity. *Mon. Weather Rev.* 129: 569–585.

Dirección General de Aguas (DGA), 2014: Cuenca del río Maipo. Gobierno de Chile.

Draxler, R.R. and Hess, G.D. (1997): Description of the HYSPLIT_4 Modeling System. NOAA Tech. Memo. ERL ARL-224, pp 24.

Gramsch, E., Cáceres, D., Oyola, P. Reyes, F., Vásquez, I., Rubio, M.A. and Sánchez, G. (2014). Influence of Surface and Subsidence Thermal Inversion on $PM_{2.5}$ and Black Carbon Concentration. *Atmos. Environ*. 9: 290–298.

Hong, SY. and Lim, J.O. (2006). The WRF Single-moment 6-class Microphysics Scheme (WSM6). *J. Korean Meteorol. Soc.* 42: 129–151.

Jhun, I., Oyola, P. Moreno, F., Castillo, M. and Koutrakis, P. (2013). $PM_{2.5}$ Mass and Species Trends in Santiago, Chile, 1998 to 2010: The Impact of Fuel-related Interventions and Fuel Sales. *J. Air Waste Manage. Assoc.* 63: 161–169.

Ménégoz, M., Krinner, G., Balkanski, Y., Boucher, O., Cozic, A., Lim, S., Ginot, P., Laj, P., Gallée, H., Wagnon, P. and Marinoni, A. (2014). Snow Cover Sensitivity to Black Carbon Deposition in the Himalayas: From Atmospheric and Ice Core Measurements to Regional Climate Simulations. *Atmos. Chem. Phys.* 14: 4237–4249.

Mlawer, E.J., Taubman, S.J., Brown, P.D., Iacono, M.J. and Clough, S.A. (1997). Radiative Transfer for Inhomogeneous Atmosphere: RRTM, a Validated Correlated-k Model for the Long Wave. *J. Geophys. Res.* 102: 16 663–16 682.

Molina, L.T., Gallardo, L., Andrade, M., Baumgardner, D., Borbor-Córdova, M., Bórquez, R., Casassa, G., Cereceda-Balic, F., Dawidowski, L., Garreaud, R., Huneeus, N., Lambert, F., McCarty, J.L., Mc Phee, J., Mena-Carrasco, M., Raga, G.B., Schmitt, C. and Schwarz, J.P. (2015). Pollution and Its Impacts on the South American Cryosphere. *Earth's Future* 3: 345–369.

Muñoz, R. and Undurraga, A. (2010). Daytime Mixed Layer over the Santiago Basin: Description of Two Years of Observations with a Lidar Ceilometer. *J. Appl. Meteorol*. 49: 1728–1741.

Nakanishi, M. and Niino, H. (2006). An Improved Mellor–Yamada Level-3 Model: Its Numerical Stability and Application to a Regional Prediction of Advection Fog. *Boundary Layer Meteorol.* 119: 397–407.

Nakayama, T., Suzuki, H., Kagamitani, S., Ikeda, Y., Uchiyama, A. and Matsumi, Y. (2015). Characterization of a Three Wavelength Photoacoustic Soot Spectrometer (PASS-3) and a Photoacoustic Extinctiometer (PAX). *J. Meteorolog. Soc. Jpn.* 93: 285–308.

Quiroz, R., Popp, P. and Barra, R. (2009). Analysis of PCB Levels in Snow from the Aconcagua Mountain (Southern Andes) Using the Stir Bar Sorptive Extraction. *Environ. Chem. Lett.* 7: 283–288.

Rabatel, A., Francou, B., Soruco, A., Gomez, J., Cáceres, B., Ceballos, J.L., Basantes, R., Vuille, M., Sicart, J.E., Huggel, C., Scheel, M., Lejeune, Y., Arnaud, Y., Collet, M., Condom, T., Consoli, G., Favier, V., Jomelli, V., Galarraga, R., Ginot, P., Maisincho, L., Mendoza, J., Ménégoz, M., Ramirez, E., Ribstein, P., Suarez, W., Villacis, M. and Wagnon, P (2013). Current State of Glaciers in the Tropical Andes: A Multi-century Perspective on Glacier Evolution and Climate Change. *The Cryosphere* 7: 81–102.

Retama, A., Baumgardner, D., Raga, G.B., McMeeking, G.R. and Walker, J.W. (2015). Seasonal Trends in Black Carbón Properties and Co-pollutants in Mexico City. *Atmos. Chem. Phys. Discuss.* 15: 12539–12582.

Saha, S., Moorthi, S., Wu, X., Wang, J., Nadiga, S., Tripp, P., Behringer, D., Hou, Y., Chuang, H., Iredell, M., Ek, M., Meng, J., Yang, R., Peña Mendez, van den Dool, H., Zhang, Q., Wang, W., Chen, M. and Becker, E. (2014). The NCEP Climate Forecast System Version 2. *J. Clim.* 27: 2185–2208.

Schmitt, C.G., All, J.D., Schwarz, J.P., Arnott, W.P., Cole, R.J., Lapham, E. and Celestian, A. (2015). Measurements of light absorbing particulates on the glaciers in the Cordillera Blanca, Peru. *The Cryosphere* 9: 331–340.

Seguel, R.J., Mancilla, C.A., Rondanelli, R., Leiva, M.A. and Morales, R.G.E. (2013). Ozone Distribution in the Lower Troposphere over Complex Terrain in Central Chile. *J. Geophys. Res.* 118: 2966–2980.

Skamarock, W.C., Klemp, J.B., Dudhia, J., Gill, D.O. Barker, D.M., Duda, M., Huang, X.Y., Wang, W. and Powers, J.G. (2008). A Description of the Advanced Research WRF Version 3. NCAR Technical Note, NCAR/TN–475+ST.

Tiedtke, M. (1989). A Comprehensive Mass Flux Scheme for Cumulus Parameterization in Large-Scale Models. *Mon. Weather Rev.* 117: 1779–1800.

Zhang, C., Wang, Y. and Hamilton, K. (2011). Improved Representation of Boundary Layer Clouds over the Southeast Pacific in ARW-WRF Using a Modified Tiedtke Cumulus Parameterization Scheme. *Mon. Weather Rev.* 139: 3489–3513.

Received for review, May 25, 2015
Revised, September 1, 2015
Accepted, September 24, 2015